Supplement of Atmos. Chem. Phys., 22, 1251–1269, 2022
https://doi.org/10.5194/acp-22-1251-2022-supplement

Atmospheric Chemistry and Physics
Open Access
EGU

Supplement of

Influence of organic aerosol molecular composition on particle absorptive properties in autumn Beijing

Jing Cai et al.

Correspondence to: Claudia Mohr (claudia.mohr@aces.su.se) and Kaspar R. Daellenbach (kaspar.daellenbach@psi.ch)

1. Method Summary

Information on the offline FIGAERO-CIMS method can be found in previous studies (Siegel et al., 2021; Huang et al., 2019). However, due to high mass loadings on our filters, we had to adjust the analytical protocol as follows:

1) "sandwich technique" to be able to only use a small punch of the filter. We took 2mm punches of our filter samples and put them between two clean pre-baked (at 200 °C for 1 hour prior to usage) originally sized (25 mm) Zefluor® Teflon filters that fit the FIGAERO filter holder. This allows to reduce the amount of desorbed PM and thus to control reagent ion depletion (shown in Figure S1).

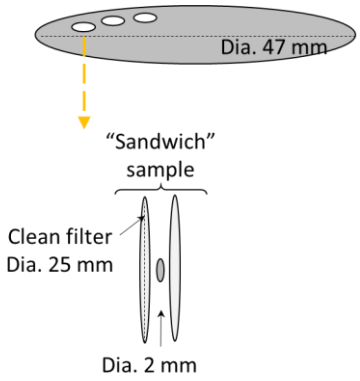

Figure S1. Schematic of the "sandwich technique" sample preparation

2) "non-uniform temperature ramping" protocol during the FIGAERO-CIMS desorption to reduce the rate of HNO_3 vaporization and thus HNO_3 signal and reagent ion depletion at temperatures between 80 and 100 °C, as following: (1) heating from room temperature (~25 °C) to 60 °C in 8 min, (2) from 60 to 110 °C in 15 min, (3) from 110 °C to 200 °C in 12 min, and (4) held at 200 °C for an additional 20 min ("soak") (shown in Figure S2).

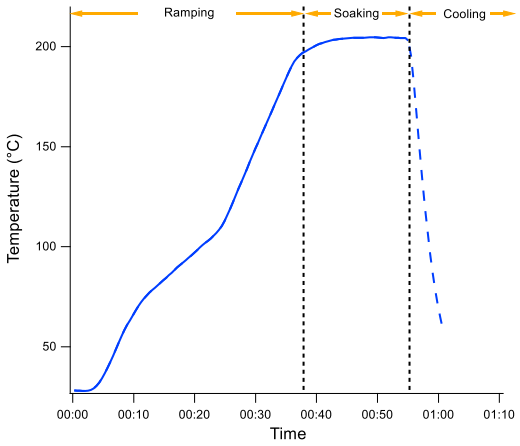

Figure S2. The FIGAERO-CIMS temperature ramping protocol applied in this study

Background subtraction method to estimate instrumental and field blanks: The variation in instrument background is taken into account using the signal at maximum heating temperature (200 °C) and thus elevated temperature of surfaces downstream

the filter. Thus, the total background signals are the field blanks (average of the 3 blanks) scaled by the signal ratios of ambient sample to blanks of the last 1.5–3 min of the soaking period."

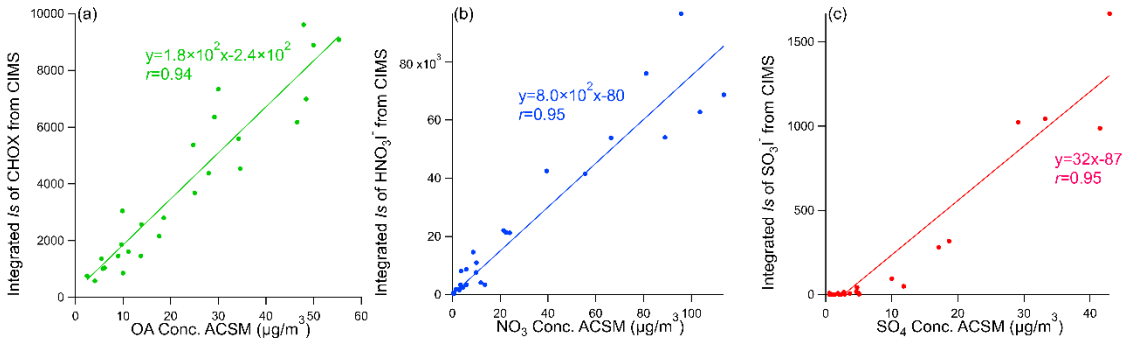

Figure S3. The comparison between signals from FIGAERO-CIMS and the concentrations of major components of $PM_{2.5}$: (a) CHOX versus OA from ACSM (b) HNO_3I^- versus NO_3 from ACSM, and (c) SO_3I^- versus SO_4 from ACSM

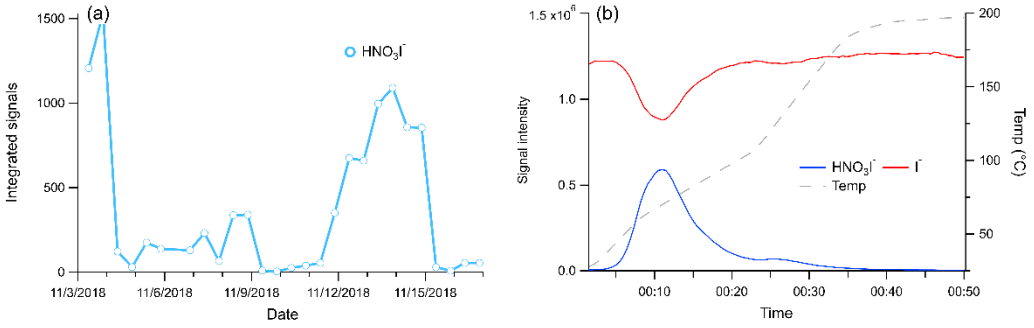

Figure S4. (a)Time series of HNO_3I^- integrated signals during the whole sampling period and (b) time series of the signals HNO_3I^-, I^- and temperature for the sample of Nov 8.

2. Aerosol water content (AWC) sensitivity tests

We assessed the uncertainty of AWC estimated by ISORROPIA II through a series of three sensitivity tests:

1) HCl: This sensitivity test uses measured gaseous HCl concentrations for estimating AWC. During the sampling period, gaseous HCl concentrations were measured by NO_3-CI-APi-TOF. The normalized HCl signals were calibrated by a comparison between NO_3-CI-APi-TOF and a co-located Monitor for AeRosols and Gases in Ambient air (MARGA; Metrohm Inc., Switzerland) after our sampling period (Sep 2 to Sep 6, 2019). The details for HCl measurements and calibration are presented in Fan et al. (2021).
2) HCl+Organonitrates: This sensitivity test is based on the HCl sensitivity test but also accounts for the contribution of particulate organic nitrates (PON) when calculating AWC. The fraction of PON to organic aerosol (OA) is estimated at 14.8% in Beijing during wintertime by a thermodenuder–aerosol mass spectrometer method (Xu et al., 2021). This fraction is also consistent with previous studies using the NO^+/NO_2^+ ratio from the AMS (Farmer et al., 2010). Thus, we used a PON/OA fraction of 14.8% and measured OA concentrations by the ACSM to estimate the concentration of PON during our sampling period. Inorganic nitrate is calculated by subtracting PON from the total NO_3 measured by ACSM. Such an assumption would provide us an upper limit contribution of PON nitrate since the mass contribution from other elements (e.g. C and H) in PON was also subtracted and further upper estimation of the AWC bias due to PON.
3) HCl+Organonitrates+Gaseous HNO_3: This sensitivity test is based on the HCl+Organonitrates sensitivity test but also accounts for gaseous HNO_3 when estimating AWC. Under the meteorological conditions during our sampling period (RH_{avg}=45%, $Temp_{avg}$= 9.2 ℃), the particle-phase fractions (ε) of NO_3 ($\varepsilon(NO_3^-)$ = (NO_3^-/(HNO_3+NO_3^-)), mol/mol)) is generally over 82% in autumn Beijing (Ding et al., 2019). The effects of gaseous HNO_3 on AWC are estimated with the assumption of $\varepsilon(NO_3^-)$ = 82% and PON/OA = 14.8%.

The AWC estimated in these three sensitivity tests agreed well with each other as well as with the base case used in the manuscript (r^2=1.0 and slope=1.0, shown in Figure R7). Therefore, we can safely draw the conclusion that gaseous HCl, HNO_3, and organonitrates do not significantly affect the AWC estimations in this study.

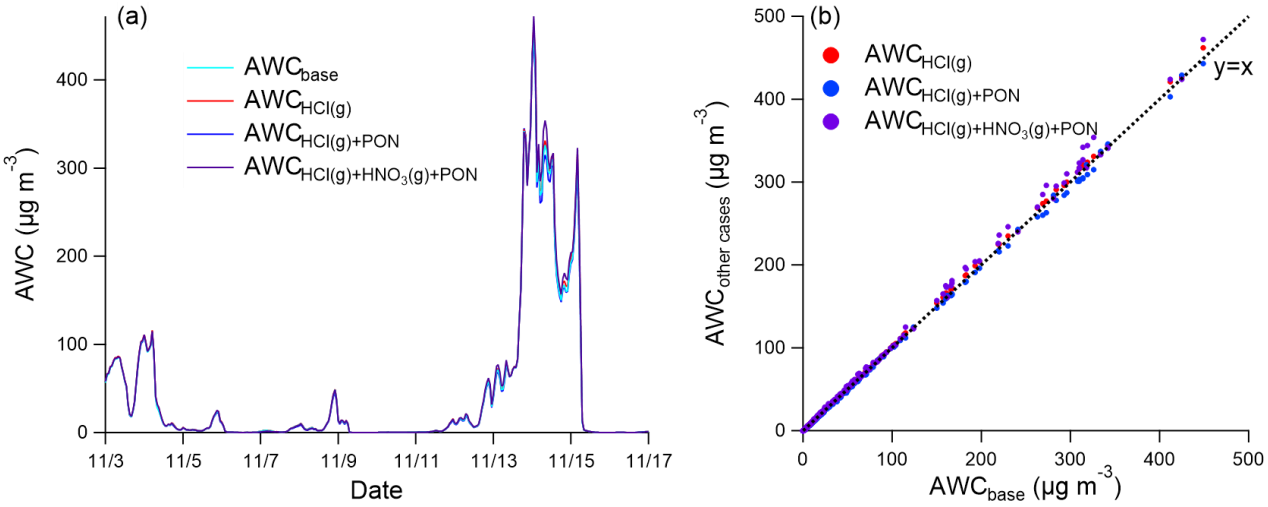

Figure S5. (a) Time series of AWC concentrations in the base case (AWC_{base}) and the three sensitivity tests: 1) including gaseous HCl ($AWC_{HCl(g)}$), 2) including gaseous HCl and organonitrate effects ($AWC_{HCl(g)+PON}$), 3) and including gaseous HCl, HNO_3, and organonitrate effects ($AWC_{HCl(g)+ HNO3(g)+PON}$), and (b) the correlation between the AWC concentrations in different cases

3. Supplementary information of the measurement and OA compositions

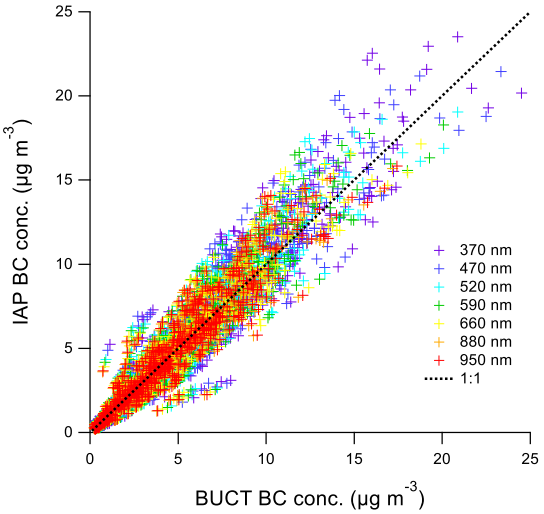

Figure S6. The correlation of BC concentrations between the IAP and BUCT site during the sampling period

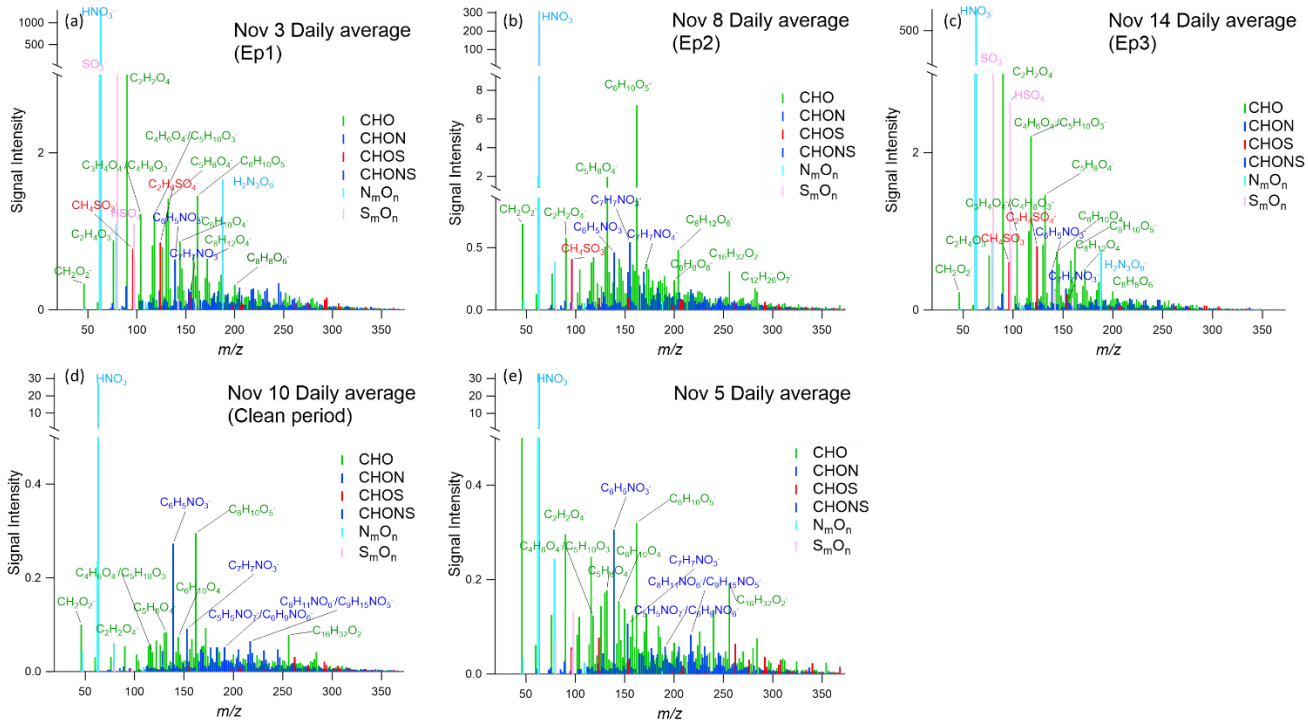

Figure S7. Daily averaged mass spectra of (a) Ep1 (Nov 3), (b) Ep2 (Nov 8), (c) Ep3 (Nov 14), (d) the clean period (Nov 10) and (e) another clean day (Nov 5)

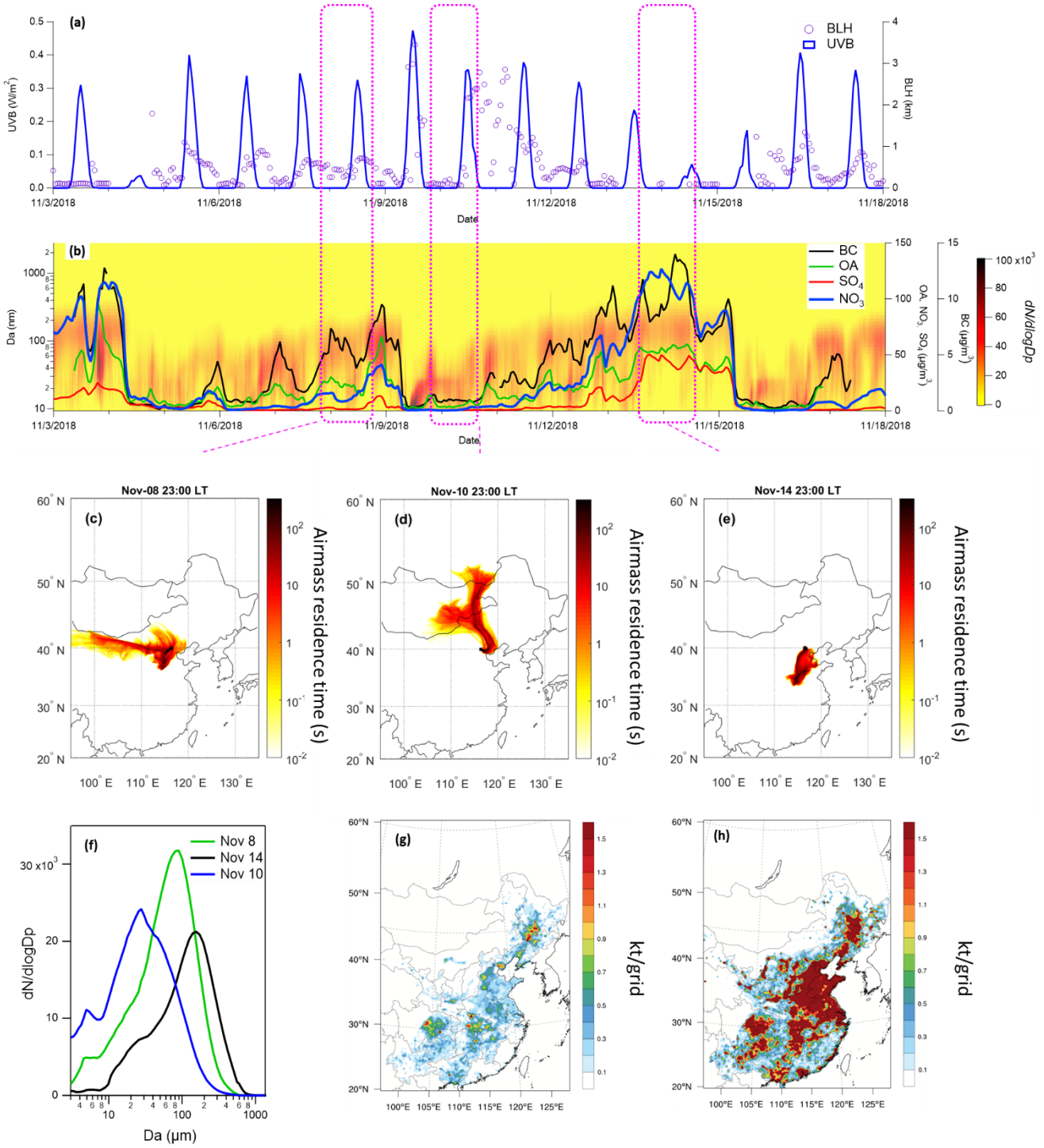

Figure S8. (a) Boundary layer and UVB, (b) particle size distribution during the sampling period measured by a co-located Particle Size Distribution System (PSD, (Liu et al., 2016; Dada et al., 2020)) as well as OA, SO_4, NO_3 measured by ACSM and BC measured by aethalometer, (c) 72-h back trajectories of Nov 8 23:00, (d) 72-h back trajectories of 23:00 Nov 10, (e) 72-h back trajectories Nov 14 23:00, (f) daily average size distribution of Nov 8, Nov 10 and Nov 14, (g) emission rate of $PM_{2.5}$ from residential emissions in East China for the year of 2015, and (h) emission rate of total $PM_{2.5}$ in East China for the year of 2015. Air mass back trajectories (retroplumes) were calculated using FLEXPART (FLEXible PARTicle dispersion model; version 9.02) (Stohl et al., 2005) with ECMWF (European Centre for Medium-Range Weather Forecasts) operational forecast data (0.15° horizontal and 1h temporal resolution) as the meteorological input. The emission rate of $PM_{2.5}$ data is from Zheng et al. (2019).

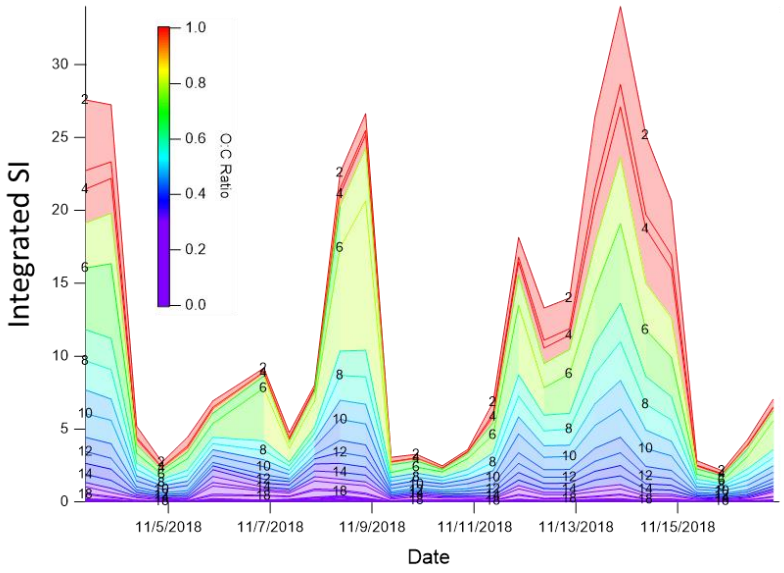

Figure S9. Time series of integrated signal intensities for different carbon number compounds. The number in the plot represents the carbon number of the compounds and the color indicates the average O:C ratios of the same carbon number compounds.

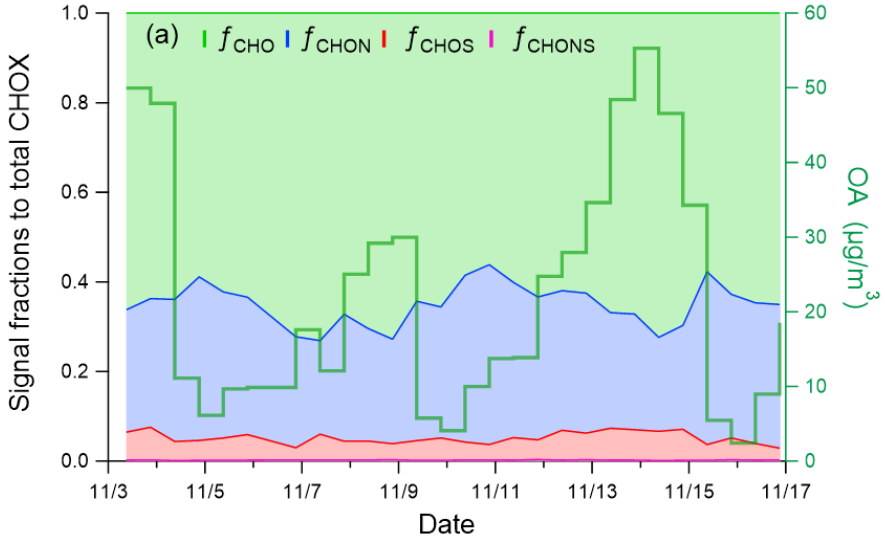

Figure S10. Time series of the fractions of CHO, CHON, CHOS and CHONS groups and OA concentration from ACSM

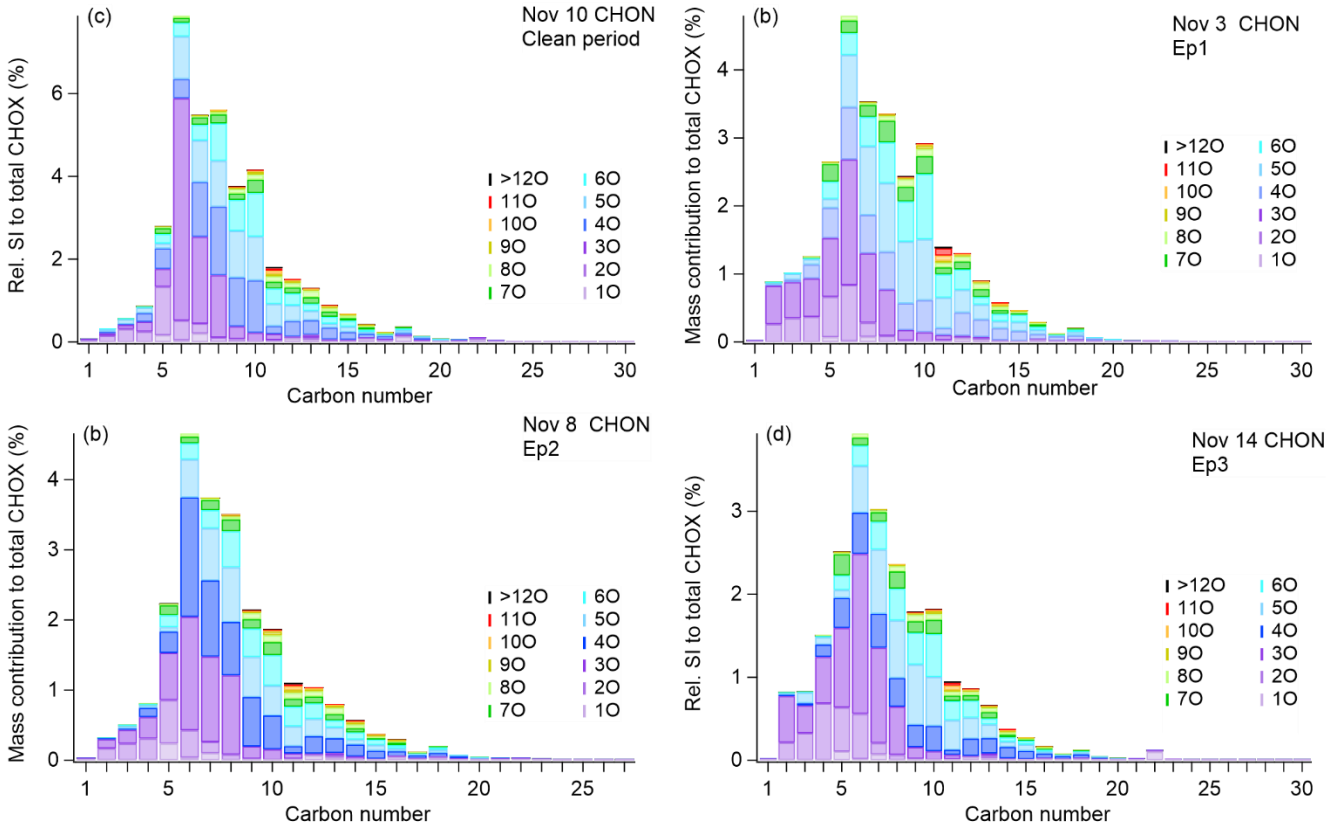

Figure S11. Signal fractions to total CHOX for CHON compounds with different numbers of oxygen and carbon atoms, (a) clean period (Nov 10), (b) Ep1 (Nov 3), (c) Ep2 (Nov 8) and (d) Ep3 (Nov 14).

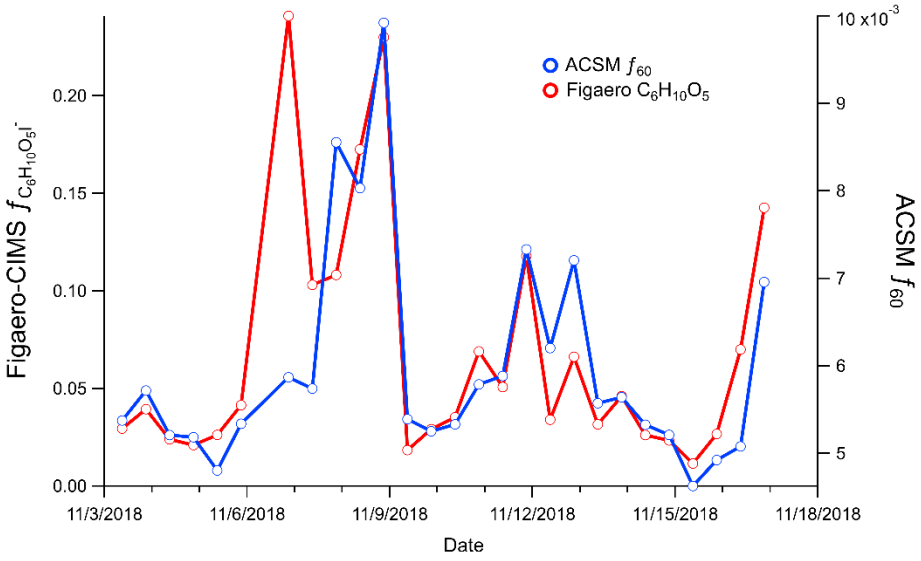

Figure S12. Time series of f_{60} from ACSM and $f_{C6H10O5I^-}$ from FIGAERO-CIMS. The discrepancy on Nov 6th is likely due to the high measurement uncertainties from the low OA concentrations (~10 μg m^{-3} and ~0.2 μ/punch).

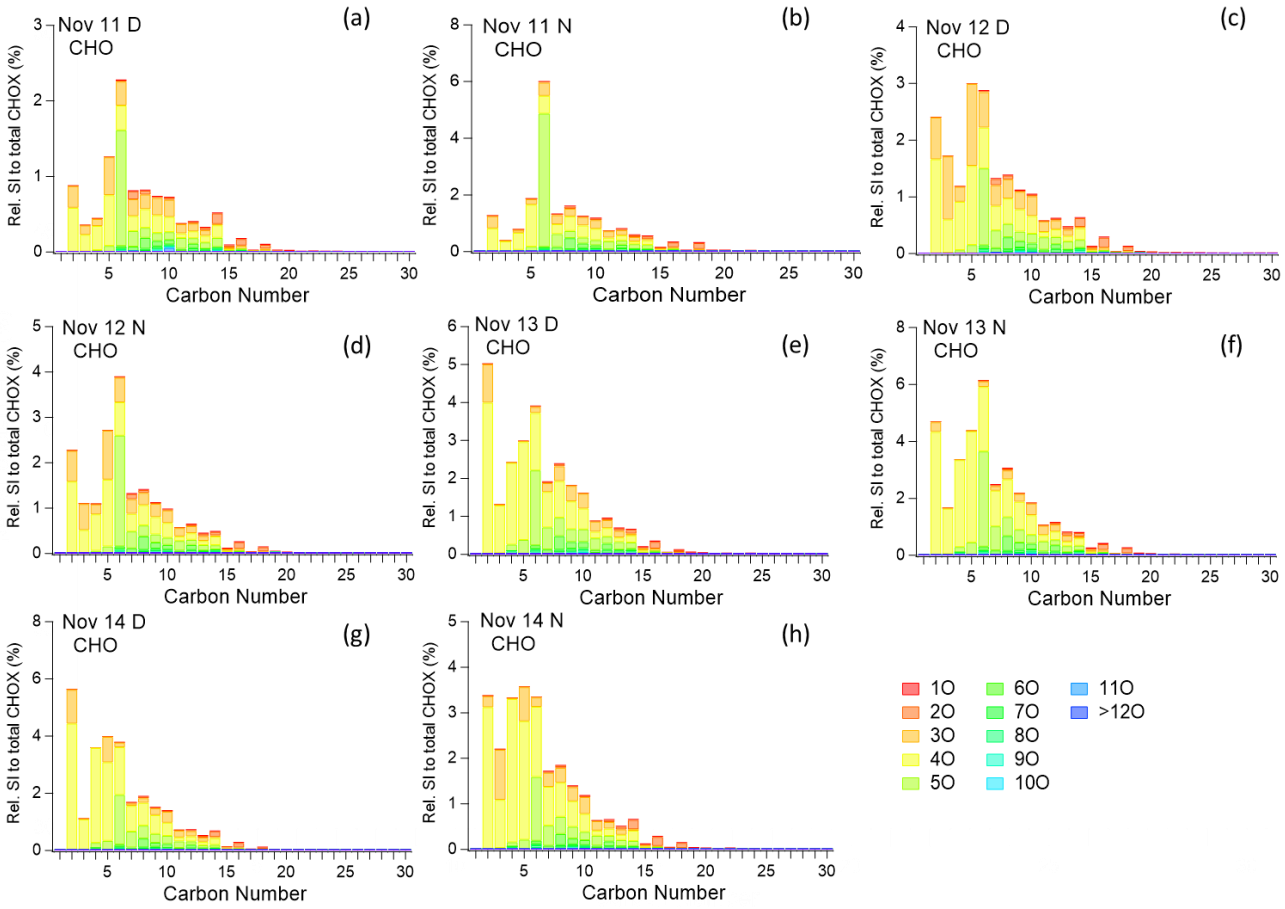

Figure S13. Signal fractions to total CHOX for CHO compounds with different numbers of oxygen and carbon atoms for (a) Nov 11 daytime, (b) Nov 11 nighttime, (c) Nov 12 daytime (d) Nov 13 nighttime, (e) Nov 13 daytime, (f) Nov 13 nighttime, (g) Nov 14 daytime, (h) Nov 14 nighttime

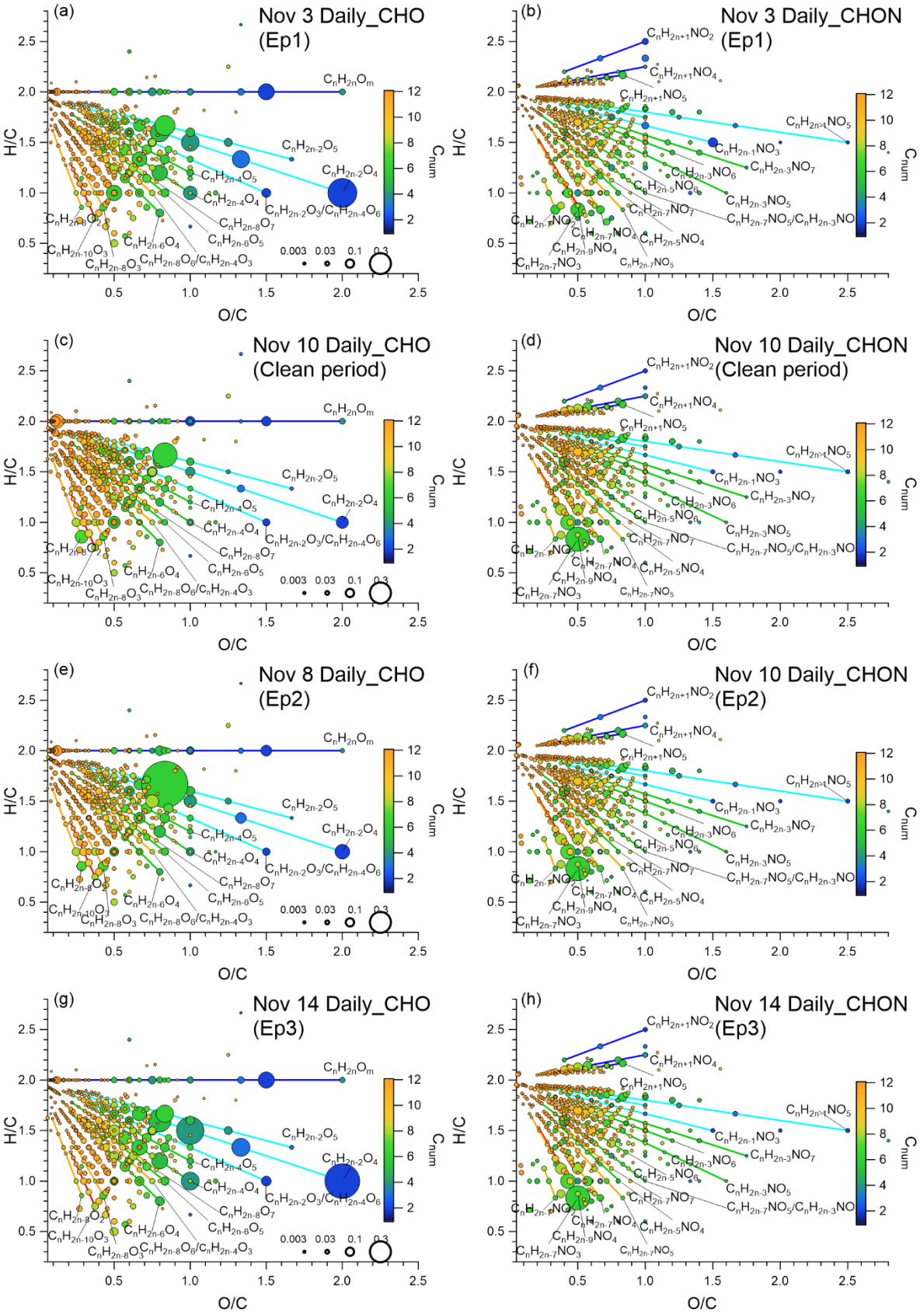
(a)
Nov 3 Daily_CHO
(Ep1)
(b)
Nov 3 Daily_CHON
(Ep1)
(c)
Nov 10 Daily_CHO
(Clean period)
(d)
Nov 10 Daily_CHON
(Clean period)
(e)
Nov 8 Daily_CHO
(Ep2)
(f)
Nov 10 Daily_CHON
(Ep2)
(g)
Nov 14 Daily_CHO
(Ep3)
(h)
Nov 14 Daily_CHON
(Ep3)
H/C
O/C
C_num
0.003 0.03 0.1 0.3

Figure S14. (a) Van Krevelen (VK) diagram of CHO compounds in Ep1 (Nov 3), (b) VK diagram of CHON compounds in Ep1 (Nov 3), (c) VK diagram of CHO compounds in the Clean period (Nov 10), (d) VK diagram of CHON compounds in the Clean period (Nov 10), (e) VK diagram of CHO compound in Ep2 (Nov 8), (f) VK diagram of CHON compound in Ep2 (Nov 8), (g) VK diagrams of CHO compound in Ep3 (Nov 14), (h) VK diagram of CHON compound in Ep3 (Nov 14). Each dot represents an identified compound with its H/C and O/C ratios and color-coded by carbon number. The size of symbols is proportional to the square root of the normalized relative signal intensity of each compound.

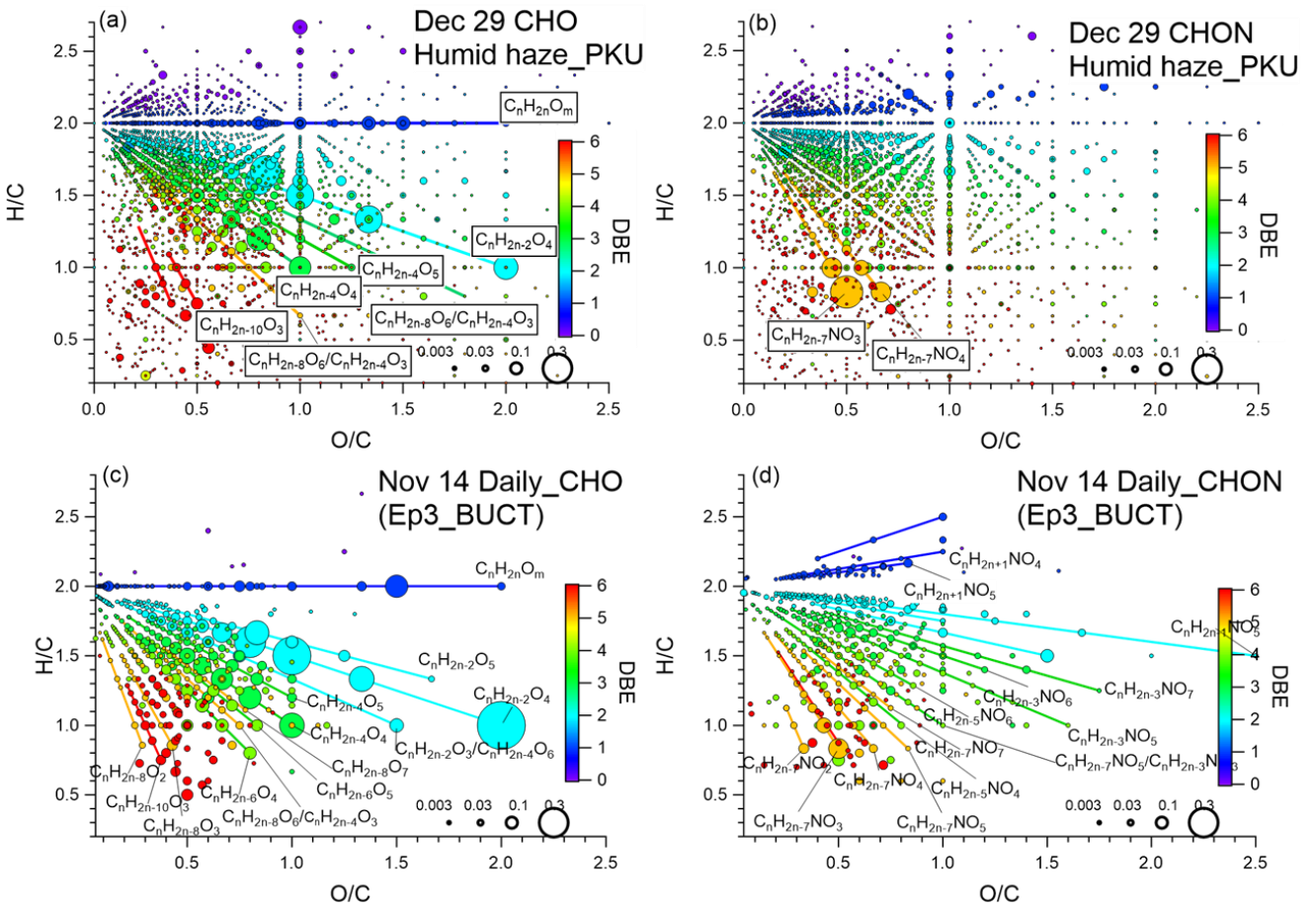

Figure S15. Comparison of identified CHO and CHON compounds in winter 2017 at PKU site and autumn 2018 at BUCT site. (a) Van Krevelen (VK) diagram of CHO compounds during haze period 2017 at PKU site, (b) VK diagram of CHON compounds during haze period 2017 at PKU site, (c) VK diagrams of CHO compounds during Ep3 (Nov 14) at BUCT site, (d) VK diagrams of CHON compound during Ep3 (Nov 14) at BUCT site. The data from PKU site is from (Zheng et al., 2021).

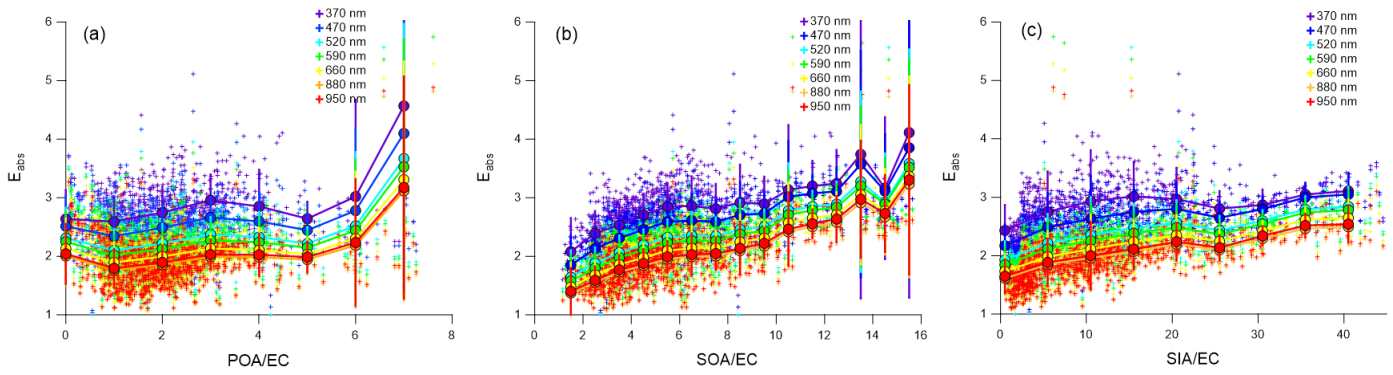

Figure S16. E_{abs} at different wavelengths as a function of (a) POA/EC, (b) SOA/EC, and (c) SIA/EC during the whole sampling period

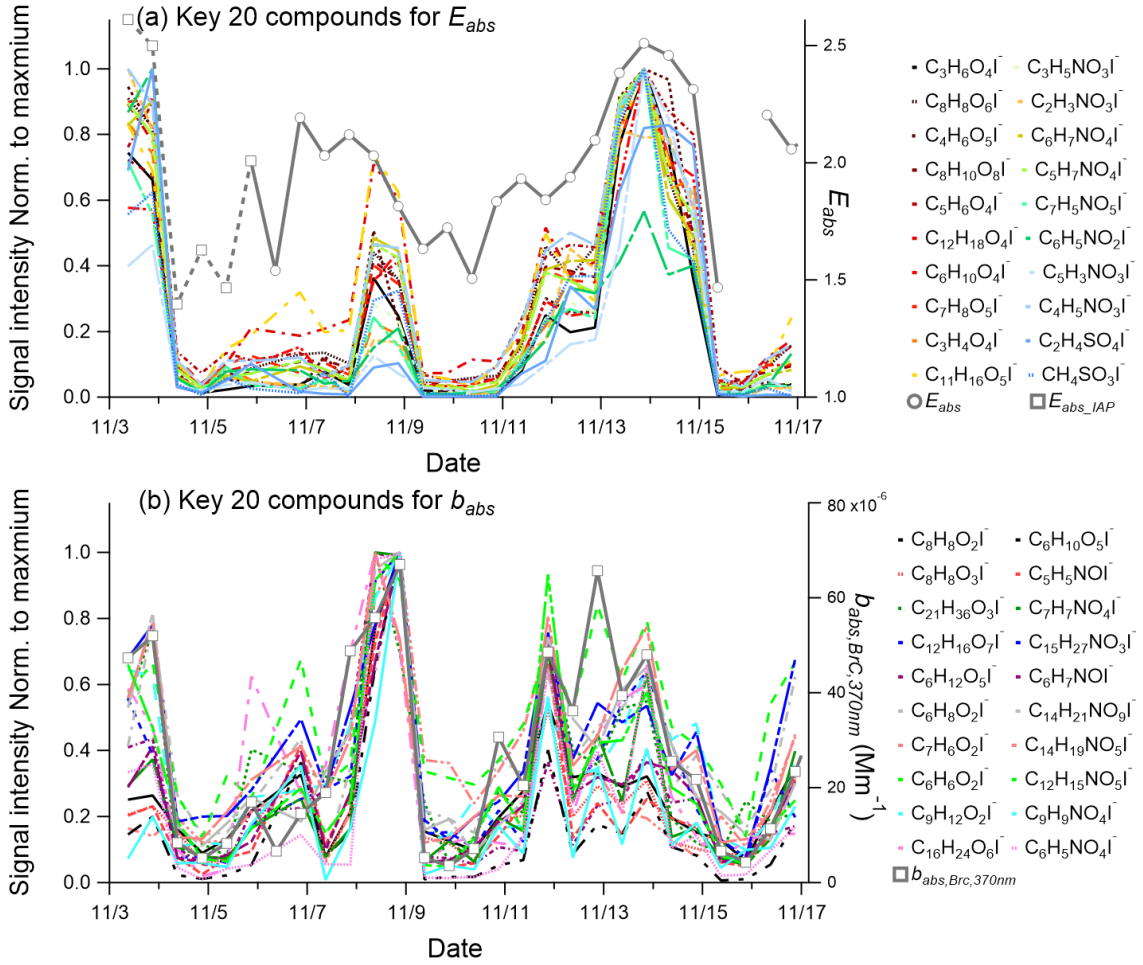

Figure S17. Normalized time series of (a) E_{abs} and key 20 compounds for E_{abs}, of (b) b_{abs} and key 20 compounds for b_{abs}.

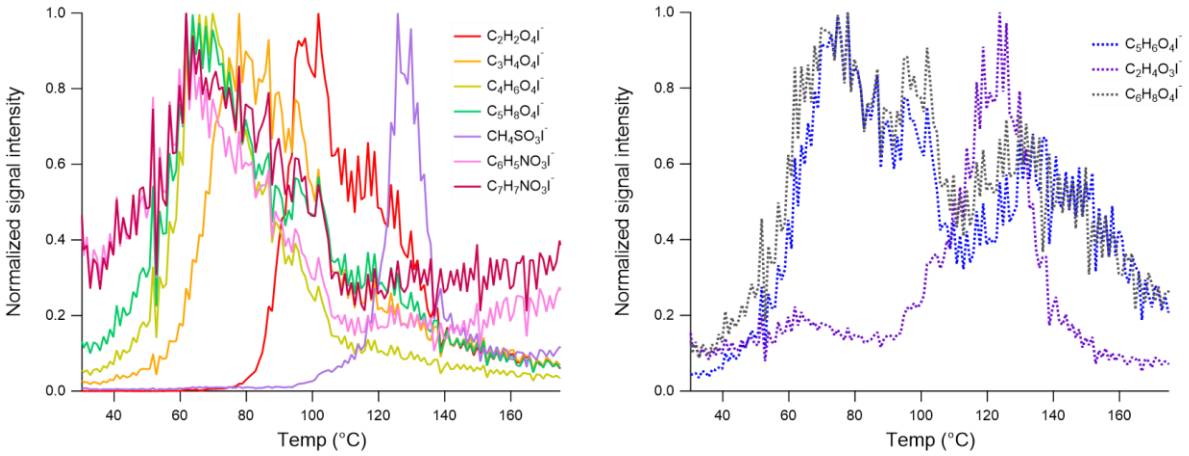

Figure S18. Normalized thermograms of the ions of (a) $C_2H_2O_4I^-$, $C_3H_4O_4I^-$, $C_4H_6O_4I^-$, $C_5H_8O_4I^-$, $CH_4SO_3I^-$, $C_6H_5NO_3I^-$, $C_7H_7NO_3I^-$ and (b) $C_5H_6O_4I^-$, $C_2H_4O_3I^-$, $C_6H_8O_4I^-$, on Nov 14. The thermograms were first corrected for the non-constant ramping rate and then normalized by the maximum signals during the desorption.

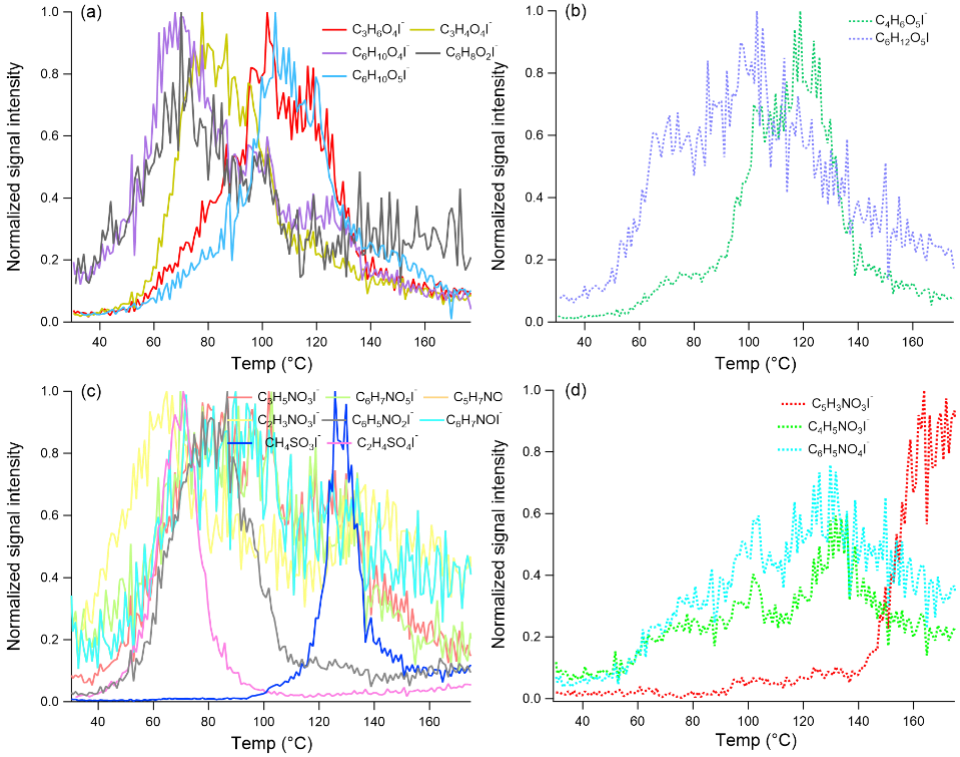

Figure S19. Normalized thermograms of the ions of the 18 key compounds on Nov 14 with $C_{num} \leq 6$ in Figure 6 (a) CHO group compounds without strong influence by thermal decompositions, and (b) CHO group compounds with a potentially strong influence by thermal decompositions, (c) CHON group compounds without strong influence by thermal decompositions and (d) CHON group compounds a potentially strong influence by thermal decompositions. The thermograms were normalized by the maximum signals during the desorption.

Table S1 Sampling information and mass loadings on the punches

Sampling date	Sampling time	NR-$PM_{2.5}$+BC loading (μg/punch)	OA loading (μg/punch)
Nov 3	9:30–21:00	3.87	1.04
	21:30–9:00	4.11	1.00
Nov 4	9:30–21:00	0.63	0.23
	21:30–9:00	0.28	0.13
Nov 5	9:30–21:00	0.61	0.20
	21:30–9:00	0.48	0.21
Nov 6	9:30–21:00	NaN	NaN
	21:30–9:00	0.57	0.37
Nov 7	9:30–21:00	0.58	0.25
	21:30–9:00	1.02	0.52
Nov 8	9:30–21:00	1.51	0.61
	21:30–9:00	1.49	0.62
Nov 9	9:30–21:00	0.17	0.12
	21:30–9:00	0.14	0.09
Nov 10	9:30–21:00	0.33	0.21
	21:30–9:00	0.49	0.29
Nov 11	9:30–21:00	0.77	0.29
	21:30–9:00	1.30	0.52
Nov 12	9:30–21:00	2.03	0.58
	21:30–9:00	2.70	0.72
Nov 13	9:30–21:00	4.84	1.01
	21:30–9:00	5.57	1.15
Nov 14	9:30–21:00	4.65	0.97
	21:30–9:00	3.43	0.71
Nov 15	9:30–21:00	0.22	0.11
	21:30–9:00	0.09	0.05
Nov 16	9:30–21:00	0.32	0.19
	21:30–9:00	0.65	0.39
Oct 26, Nov 4, Nov 17 (blanks)			

Note: Field blanks were collected by putting in the sample holder for 10 minutes without activating the sampling flow and were later analyzed the same method as the samples

Table S2 Comparison of absolute integrated signal (*Is*) of some major compounds for different episodes

ions	Absolute *Is* (count) Ep1	Ep2	Ep3	Clean
HNO_3I^-	1381	337	854	30
SO_3I^-	3.96	0.10	13.32	0.02
$CH_4SO_3I^-$	1.00	0.48	0.79	0.01
$C_2H_4SO_4I^-$	0.92	0.11	0.86	0.00
$C_2H_2O_4I^-$	3.45	0.58	3.85	0.05
$C_3H_4O_4I^-$	1.22	0.29	0.97	0.01
$C_4H_6O_4I^-$	1.25	0.41	2.35	0.03
$C_5H_8O_4I^-$	1.57	1.99	1.62	0.12
$C_6H_{10}O_5I^-$	1.86	8.51	0.91	0.51
$C_6H_5NO_4I^-$	0.22	0.60	0.08	0.03
$C_7H_7NO_4I^-$	0.12	0.33	0.05	0.05

Reference

Dada, L., Ylivinkka, I., Baalbaki, R., Li, C., Guo, Y., Yan, C., Yao, L., Sarnela, N., Jokinen, T., Daellenbach, K. R., Yin, R., Deng, C., Chu, B., Nieminen, T., Wang, Y., Lin, Z., Thakur, R. C., Kontkanen, J., Stolzenburg, D., Sipilä, M., Hussein, T., Paasonen, P., Bianchi, F., Salma, I., Weidinger, T., Pikridas, M., Sciare, J., Jiang, J., Liu, Y., Petäjä, T., Kerminen, V.-M., and Kulmala, M.: Sources and sinks driving sulfuric acid concentrations in contrasting environments: implications on proxy calculations, Atmospheric Chemistry and Physics, 20, 11747-11766, 10.5194/acp-20-11747-2020, 2020.

Ding, J., Zhao, P., Su, J., Dong, Q., Du, X., and Zhang, Y.: Aerosol pH and its driving factors in Beijing, Atmospheric Chemistry and Physics, 19, 7939-7954, 10.5194/acp-19-7939-2019, 2019.

Fan, X., Cai, J., Yan, C., Zhao, J., Guo, Y., Li, C., Dällenbach, K. R., Zheng, F., Lin, Z., Chu, B., Wang, Y., Dada, L., Zha, Q., Du, W., Kontkanen, J., Kurtén, T., Iyer, S., Kujansuu, J. T., Petäjä, T., Worsnop, D. R., Kerminen, V.-M., Liu, Y., Bianchi, F., Tham, Y. J., Yao, L., and Kulmala, M.: Atmospheric gaseous hydrochloric and hydrobromic acid in urban Beijing, China: detection, source identification and potential atmospheric impacts, Atmospheric Chemistry and Physics, 21, 11437-11452, 10.5194/acp-21-11437-2021, 2021.

Farmer, D. K., Matsunaga, A., Docherty, K. S., Surratt, J. D., Seinfeld, J. H., Ziemann, P. J., and Jimenez, J. L.: Response of an aerosol mass spectrometer to organonitrates and organosulfates and implications for atmospheric chemistry, Proc Natl Acad Sci U S A, 107, 6670-6675, 10.1073/pnas.0912340107, 2010.

Huang, W., Saathoff, H., Shen, X., Ramisetty, R., Leisner, T., and Mohr, C.: Seasonal characteristics of organic aerosol chemical composition and volatility in Stuttgart, Germany, Atmospheric Chemistry and Physics, 19, 11687-11700, 10.5194/acp-19-11687-2019, 2019.

Liu, J., Jiang, J., Zhang, Q., Deng, J., and Hao, J.: A spectrometer for measuring particle size distributions in the range of 3 nm to 10 μm, Frontiers of Environmental Science & Engineering, 10, 63-72, 10.1007/s11783-014-0754-x, 2016.

Siegel, K., Karlsson, L., Zieger, P., Baccarini, A., Schmale, J., Lawler, M., Salter, M., Leck, C., Ekman, A. M. L., Riipinen, I., and Mohr, C.: Insights into the molecular composition of semi-volatile aerosols in the summertime central Arctic Ocean using FIGAERO-CIMS, Environmental Science: Atmospheres, 10.1039/d0ea00023j, 2021.

Stohl, A., Forster, C., Frank, A., Seibert, P., and Wotawa, G.: Technical note: The Lagrangian particle dispersion model FLEXPART version 6.2, Atmos. Chem. Phys., 5, 2461-2474, 10.5194/acp-5-2461-2005, 2005.

Xu, W., Takeuchi, M., Chen, C., Qiu, Y., Xie, C., Xu, W., Ma, N., Worsnop, D. R., Ng, N. L., and Sun, Y.: Estimation of particulate organic nitrates from thermodenuder–aerosol mass spectrometer measurements in the North China Plain, Atmospheric Measurement Techniques, 14, 3693-3705, 10.5194/amt-14-3693-2021, 2021.
Zheng, H., Cai, S., Wang, S., Zhao, B., Chang, X., and Hao, J.: Development of a unit-based industrial emission inventory in the Beijing–Tianjin–Hebei region and resulting improvement in air quality modeling, Atmospheric Chemistry and Physics, 19, 3447-3462, 10.5194/acp-19-3447-2019, 2019.
Zheng, Y., Chen, Q., Cheng, X., Mohr, C., Cai, J., Huang, W., Shrivastava, M., Ye, P., Fu, P., Shi, X., Ge, Y., Liao, K., Miao, R., Qiu, X., Koenig, T. K., and Chen, S.: Precursors and Pathways Leading to Enhanced Secondary Organic Aerosol Formation during Severe Haze Episodes, Environmental Science & Technology, 10.1021/acs.est.1c04255, 2021.